Int J Adv Manuf Technol (2017) 91:227–235
DOI 10.1007/s00170-016-9738-2

ORIGINAL ARTICLE

Numerical study of welding simulation and residual stress on butt welding of dissimilar thickness of austenitic stainless steel

Jie Xia[1] · **Hui Jin**[1]

Received: 6 July 2016 / Accepted: 7 November 2016 / Published online: 18 November 2016

Abstract Weld-induced residual stress inevitably exists in the vicinity of the weld bead and may have a deleterious effect on the weld joint. In the shipyard industry, butt welds of dissimilar thickness plates are a widely used welding geometry type. Predicting the magnitude and distribution of residual stress and distortion are of significance in the design of structural components. In this work, a fusion welding simulation is studied and verified by coupling thermal-mechanical analysis, and the 'full-elastic element' technique is introduced in simulation model to improve the convergence of nonlinear calculations The prediction of weld-induced residual stress on the butt weld between similar and dissimilar thicknesses of steel plates is performed by thermal elastic-plastic finite element (FE) analysis. This exploration predicts the process of thermal cycle loads acting on the weld components as well as residual stress states. The results conclude that the geometry of weld joints significantly affects the residual stress distribution and magnitude, which presents some challenges to tolerance in structural design.

Keywords Butt-welded plate · Dissimilar thickness · Residual stress · Finite element simulation · Austenitic stainless steel

✉ Hui Jin
jinhui@seu.edu.cn

[1] Key Laboratory of Concrete and Prestressed Concrete Structures of Ministry of Education, Jiangsu Key Laboratory of Engineering Mechanics, School of Civil Engineering, Southeast University, Nanjing 210096, China

1 Introduction

Welding is a significant fabrication technique for structure connection in structural design and construction, because it is convenient and affordable for many types of complicated structures and materials. However, it also presents a number of difficult problems to the manufacturing community. Unexpected failure may occur since the residual stresses (RS) are combined with external loadings acting on materials and components, together with the presence of unknown defects or a poor microstructure, which have dangerously effect on the safety and integrity of welded structures in service. Therefore, RS often plays a determine role in different failure mechanisms [1]. Butt welding of dissimilar thickness plates is an ordinary type of welding geometry in the design practice, especially in shipyards. Weld-induced RS and distortions have significant influence on the fatigue life of a welded structure. Knowledge of weld-induced RS and distortions is necessary to meet accuracy and tolerance requirements of structural design.

Based on the thermal elastic-plastic FE method, the history of the simulation of the welding process dates back to the 1970s [2]. Many studies have been published over the past years. Deng and Murakawa [3] predicted welding distortion and RS in steel butt-welded joints by finite element simulation. The simulation result was verified by performing experiments. Lee and Chang [4] studied the effect of yield stress of base material on the magnitude and distribution of RS and carried out stress behavior in welding joints acting on superimposed tensile loads. Investigations on steel plate butt-welded joints between dissimilar base materials were also performed to further understand the RS formation and the influence of material properties [5, 6]. Choobi et al. [7] conducted the effect of clamping and clamp time on the welding RS and distortion in butt-welded of stainless steel plates. The

influence of the geometry of base material and welding parameters were revealed by Choobi [8]. Ranjbarnode et al. [9] simulated the welding process of butt-welded plates between carbon steel and stainless steel considering the effect of heat input. Heat source modeling based on arc physics was developed by Okano et al. [10] for more accurate numerical simulations of the welding process. For the medium and thick plate welding with full penetration, Ye et al. [11] established the computational approach to conduct the effect of groove type on welding RS and angular distortion. 'V', 'K', and 'X' groove joints were studied using the proposed computational procedure. The results provided some recommendations on the groove design of weld joints between thick steel plates. Singh et al. [12] proposed an adaptive volumetric heat source to simulate the welding process. The size and shape of a volumetric heat source are not formed immediately at the outset of welding. Therefore, the geometric parameters defining the size and shape should not be defined at the beginning of calculation but obtained by solving the governing heat conduction equation and boundary condition through iteration. Suzuki et al. [13] simulated the welding of 35-mm-thick dissimilar metal butt welds between ferritic and austenitic steel. The influence of thermal expansion coefficients and material strength was described in their work. The results showed good agreement with the experimental data obtained by neutron diffraction. The mechanical-properties relationships of dissimilar weld joint were investigated by spot welding [14]. The influence of the weld metal on RS and deformation were carried out to further understand the knowledge of weld joints [15]. Sun et al. [16] comparatively studied the weld-induced RS and distortion in thin-plate joints welded by laser beam welding and CO_2 gas arc welding, and revealed that smaller RS and deformation can be obtained by laser beam welding techniques. Deng et al. [17] developed a computational method to simulate the welding process of electro slag welding, and predicted the RS and distortion of thick plate joints performed by electro slag welding. The results concluded that larger angular deformation and the range of the heat affect zone may be caused by electro slag welding because the larger heat input. There are extensive literatures on these topics, such as investigations on welding techniques parameters, geometry structure, base material properties, and groove type of welding joints. However, most researches were performed on butt welds with similar thickness plates, while less attention has been paid to the dissimilar plates [18]. Although the angular distortion of welding joints between dissimilar steel plates was described by Hashemzadeh et al. [18], weld-induced RS and the effect of geometric type of weld joints were not presented. Because of the significant influence of welding RS on the fatigue and reliability of welded structures and the great challenge of measurement in practice, the welding RS in butt welds of dissimilar thickness austenitic stainless steel plates was presented in this study. Two typical types of weld joints are performed in this paper, and the influences of geometric types of weld joints are deduced by finite element methods in subsequent work. The result provides further knowledge on the mechanical property of weld joints of dissimilar thickness plates, and contributes to the fatigue design of this type of welded structure.

2 Theoretical aspects of computational welding mechanics

2.1 Coupling of thermal-mechanical analysis

According to the Fourier heat transfer theorem and energy conservation theorem, the governing equation for nonlinear thermal analysis can be established. The temperature field will change with time and spatial plates in the welding process, and the transient temperature field $T(x, y, z, t)$ can be expressed by the following equation (Eq. (1)):

$$k_x \frac{\partial^2 T}{\partial x^2} + k_y \frac{\partial^2 T}{\partial y^2} + k_z \frac{\partial^2 T}{\partial z^2} + \rho Q = \rho c_T \frac{\partial T}{\partial t} \tag{1}$$

where ρ is density, c_T is the specific heat, $k(k_x = k_y = k_z)$ is the thermal conductivity, and$Q$ is the rate of internal heat of generation.

Heat exchange between the surface of the welded structure and its surroundings occurs during welding; the dynamic boundary conditions allow for both convection and radiation. Since there are convection losses for lower temperatures away from the weld pool and radiation losses are dominating for higher temperature in the vicinity of weld, a temperature-dependent combined boundary is adopted here. The equations of heat transfer coefficient α_h are expressed as (Eq. (2)) [19]:

$$\alpha_h = \begin{cases} 0.0668 \cdot T \quad \left(W \cdot m^2\right) & 0 < T < 500 \\ 0.213 \cdot T - 82.1 \quad \left(W \cdot m^2\right) & T > 500 \end{cases} \tag{2}$$

where Trepresents the current temperature. The latent heat of fusion has been incorporated into the thermal model due to the solidification of the weld pool.

In this study, the moving welding arc is assumed as a volumetric heat source by a double ellipsoid model proposed by Goldak et al. [20]. Figure 1 depicts the double ellipsoidal heat source model. The volumetric heat flux is distributed over the whole volume of the ellipse in a Gaussian manner. The maximum flux is at the center, gradually reducing in a non-uniform manner to the edges of the ellipse. One advantage of this model is that it gives a steeper temperature gradient at the front of the heat source and smoother gradient at the rear side, which is similar to real arc wending as well as GMAW.

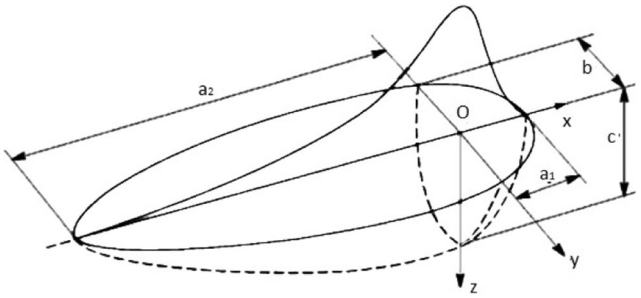

Fig. 1 Goldak double ellipsoid model

The power density distribution inside the front quadrant ellipsoidal heat source is given by the following:

$$q(x,y,z,t) = \frac{6\sqrt{3}f_f\Phi}{\pi^{3/2}a_1^2c} e^{-3(x+vt)^2/a_1^2} e^{-3y^2/b^2} e^{-3z^2/c^2} \quad (3)$$

Similarly, the power density distribution inside the rear quadrant ellipsoidal heat source is given by the following:

$$q(x,y,z,t) = \frac{6\sqrt{3}f_r\Phi}{\pi^{3/2}a_2^2c} e^{-3(x+vt)^2/a_2^2} e^{-3y^2/b^2} e^{-3z^2/c^2} \quad (4)$$

in which f_f and f_r represent the fractions of the heat deposited in the front and rear quadrants, and where $f_f + f_r = 2$. In this paper, f_f is assumed to be 1.4 and f_r is 0.6; thus, the temperature gradient in the front leading part is steeper than the back part. The parameters a_1, a_2, b, and c represent the size of the geometric shape of the heat source model. The power of welding heat source is Φ, and it can be calculated ($\Phi = \eta UI$), where U is the arc voltage and I is the welding current. The arc efficiency is η, because heat loss is inevitable in the welding process. The arc efficiency of GMAW is considered as 70% in the present study [21].

A austenitic SUS304 stainless steel is used in this study, and the temperature-dependent thermo-mechanical properties were detailed in ref. [18]. The effect of phase transformation is not taken into account for the welding simulation, because the metallurgical transformation has litter influence in austenitic stainless steel. However, significant effect on weld-induced RS may occur in welding between high strength steels [22].

The elastic part of strain and other inelastic strain components are accounted in this analysis. The total strain tensor is calculated based on the following additive decomposition relation:

$$\varepsilon_{tot} = \varepsilon_e + \varepsilon_p + \varepsilon_{th} \quad (5)$$

in which, ε_{tot} is the total strain rate, ε_e is the elastic strain rate, ε_p is the plastic strain rate due to the rate-independent plasticity, and ε_{th} is the thermal strain rate.

2.2 Simulation technique of weld metal deposition

There are two approaches to model the addition of the weld metal, namely, the quiet element and inactive element [23]. In this study, the birth and death element is applied to simulate the weld filler deposition with time. The elements belonging to the weld metal are removed at the start of analysis. When the welding torch arrives at these elements, they recover their stiffness and material properties gradually in the model with no record of strain history. The effect of filler elements addition on the analysis result is considered for calculation, because the boundary conditions on the surface of the welded structure would change with the deposition of filler elements. However, the nonconsecutive distortion may occur in new added elements belonging to weld fillers immediately adjacent to the base material elements (Fig. 2a). Since the material properties are very low (such as elastic modules) at high temperature, some error-elements may appear due to excessive distortion of those filler elements near the heat source. Both factors may bring no convergence result for nonlinear thermal analysis of welding simulation, especially for large deformation FE analysis.

In this paper, 'full-elastic element' is introduced in the process of welding simulation by ABAQUS software. Those elements belonging to weld fillers were first copied as additional elements with full-elastic material properties that are sufficiently low but lead to an ill-conditioned stiffness matrix in the FE model. As the torch arrives, the elements with filler material properties will be reactive in the appropriate

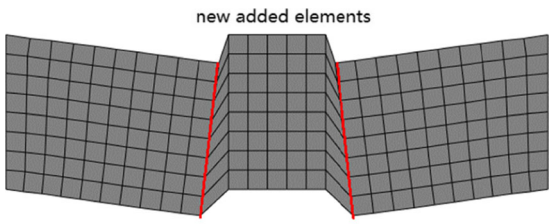

(a) Inconsecutive distortion for new added elements

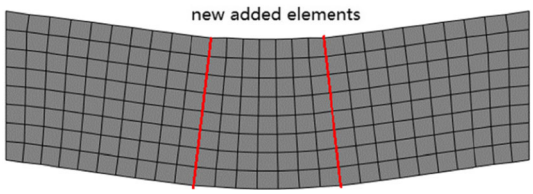

(b) Added new elements in appropriate geometric shape

Fig. 2 Modeling for weld metal deposition

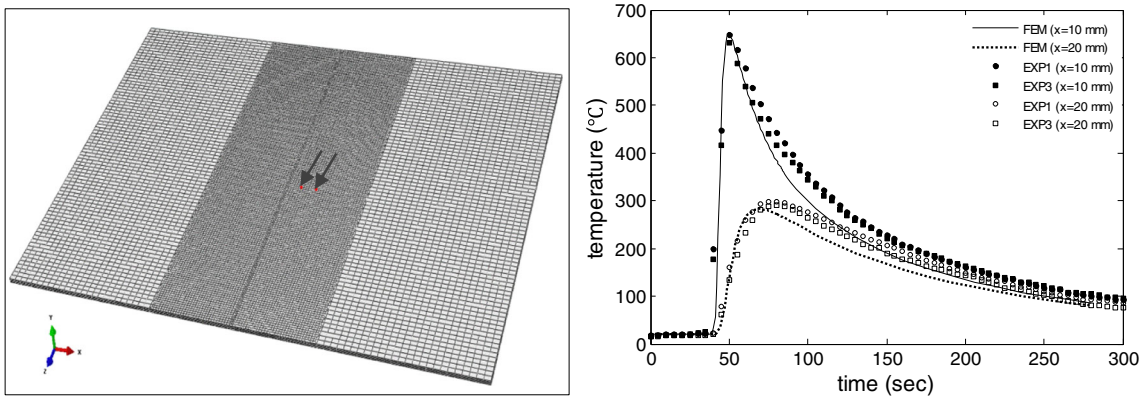

(a) FE model (b) FE and experimental temperature histories

Fig. 3 The comparison of measured data with simulated results for the welding plate

geometric shape to adjust to the deformed structure without initial strain (Fig. 2b), which can be realized by 'full-elastic element'. This applied method avoids the singular deformation of elements adjacent to the interface between filler metal and base material and excessive distortion of the newly added elements in the vicinity of the heat source. This technique greatly improves the ability to obtain a convergence solution.

3 Verification of the numerical FE model

The validity of established FE analysis methods is confirmed in this section from the experimental work by Choobi [8] in which the single-pass butt welding of steel plates with a length of 200 mm, width of 150 mm, and thickness of 2 mm was conducted, and the temperature field distributions were measured and directly compared to the FE results. The same welded structure and welding technique are performed in this section by an established FE model (Fig. 3a). The specific details can be found elsewhere [8], and his experimental measurements that were carried out on the weld specimen are superimposed on Fig. 3b and compared with the FE results by the numerical method in this paper.

The thermal cycles at different locations with respect to the time under single welding are depicted in Fig. 3b. The measuring locations are pointed out by dark arrows in Fig. 3a. The FE results are in good agreement with measured data in overall trends. Therefore, the FE method used here is verified as appropriate to the analysis of welding residual stresses.

4 Analysis of weld joints

4.1 Finite element models of welded joints

Two typical types of welding joints of dissimilar thickness plates are investigated in this paper, and compared with the butt welding joint of similar thickness plates. The geometric FE models are presented in Fig. 4. The steel plates are welded in a single-pass 'V' groove type welding joint. The welding geometric structure with joint type 2 and its details are depicted in Fig. 5. To weld the dissimilar thickness of steel plates, the thick plate is often fabricated with a transition region. The thickness in this region is gradually reduced in a limited range. The size of the transition part in width direction is 12 mm; the slope ratio in the transition region is 1:4.

The geometric parameters defining the size of the welded structure are detailed in Table 1. The length of both sides of the steel plates is 180 mm, width is 80 mm, the thickness of thin plate is 3 mm, and the other is 6 mm. As is shown in Fig. 4, the thickness of plates on both sides of the first type of weld joint (type 1) is

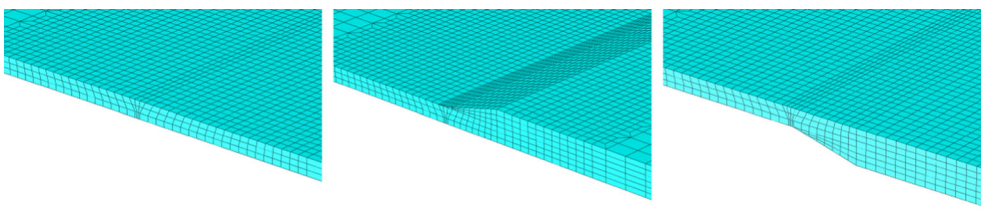

(a) Weld joint type 1 (b) Weld joint type 2 (c) Weld joint type 3

Fig. 4 The geometric structure of three types of welding joints

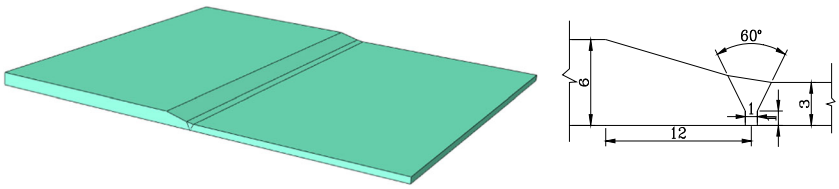

Fig. 5 The geometric structure of welding joint type 2

3 mm, as well as the plates located to the left side of the other two types of weld joints (type 2 and type 3 in Fig. 4); that of the right side is 6 mm.

SUS304 stainless steel is used in this study, and all the base materials have the same temperature-dependent thermo-mechanical parameters detailed in ref. [18]. It is presumed that weld metal has similar material properties other than the yield strength. In the welding process, the temperature-dependent yield stresses are considered in the calculation as well as the effect of strain hardening on the yield strength. Since the heat source acts on the small part of the welded structure, fine mesh is necessary in order to obtain the more accurate temperature field distribution. The arc voltage is 15 V, the electric current is 180 A, and the welding speed is 3 mm/s.

Coupling thermal-mechanical analysis is carried out in this study, so the boundary conditions for thermal analysis and mechanical analysis should be predefined. The ambient temperature is defined as 20 °C and is an initial boundary condition for thermal analysis.

4.2 Analysis of the temperature field

Figure 6 shows the thermal cycles at different locations on the surface of plate in a welded structure with joint type1. The temperature history at the locations with different distances away from the weld centerline can be found in this figure. As the figure depicts, a steeper temperature gradient occurs at the heating period and is smoother at the cooling stage, because the welding speed is often faster than the rate of heat transfer in base material. When the moving heat source is closest to these locations, the temperature peak value can be obtained.

The cooling rate is a key factor in welding technology because it has a significant influence on the weld-induced RS as well as the microstructure. Therefore, the thermal cycle load may provide important knowledge to understand and evaluate the welding structure. It can be deduced that different locations on the welded structure may be subjected to different thermal cycle loads; a place farther away from the weld centerline may undergo a lower effect of thermal cycle load.

Because the same material properties are on both sides of the weld bead and geometric structure, the axis-symmetrical temperature field distribution is obtained from the FE model (Fig. 7). Since the dominating effect of the temperature field is on the mechanical analysis, the welding RS field distribution is also axis-symmetrical with respect to the weld centerline.

4.3 Analysis of weld-induced RS

Because of differential heating and cooling, thermal stress in the weld region and its immediate vicinity leads to elastic-plastic deformation of the welded structure. The heat affect zone (HAZ) and the adjacent region undergo higher temperatures than that of farther areas of base metal. As the weld puddle solidifies and shrinks, the shrinkage stress may be exerted in surrounding weld metal and the HAZ. Compressive stress begins to exist in the relatively farther and colder areas due to the thermal expansion of hot metal in HAZ when the weld pool is formed. The tensile stress occurs during the cooling period because the contraction of weld metal and restriction of the colder base metal.

For the weld joint of dissimilar thickness plates, some special fabrication techniques should be carried out in the welding process. Figure 4 shows the two typical types of weld joints (type 2 and type 3) used to weld dissimilar thickness

Table 1 The geometric structural parameters on the FE models

	Type 1	Type 2	Type 3
Thickness (mm)	3/3	3/6	3/6
Width (mm)	80	80	80
Length (mm)	180	180	180

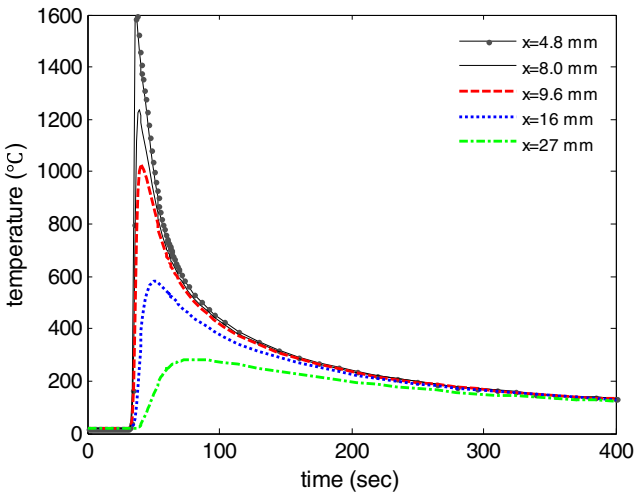

Fig. 6 Thermal cycle at five locations on the top of stainless plate for weld joint type 1

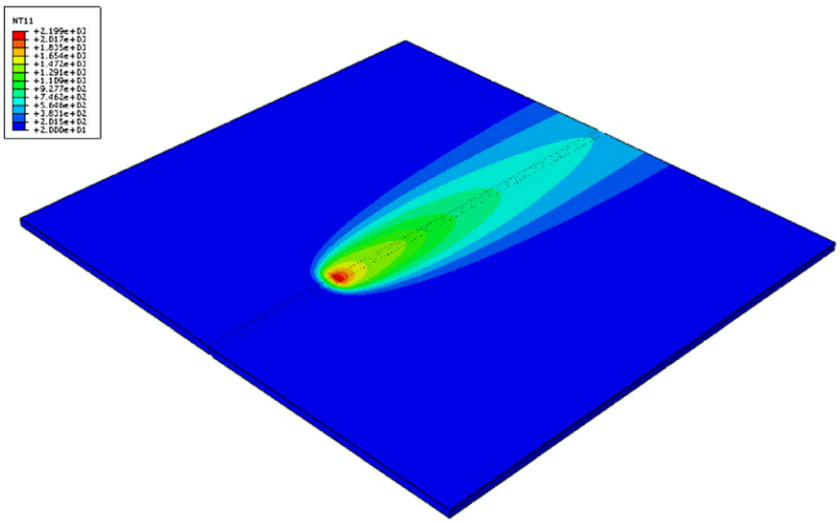

Fig. 7 Temperature field distributions on the steel plate of weld joint type 1

plates [21]. FE analysis is performed to predict the RS and distortion of two types of welded connections. The effects of geometric types of welded joints are comparatively studied in this section. Longitudinal RS is mainly presented in this paper due to its dominating danger to the integrity of the structure among the RS components. It is also a significant factor that induces fatigue crack growth into the base material from the weld metal.

The longitudinal RS of 'V' groove butt-welded joints of steel plates of similar and dissimilar thickness are depicted in the following figures. Figures 8 and 9 portray the distributions and magnitudes of longitudinal RS on the surfaces of plates located on two sides of the weld bead. Tensile RS exerts in HAZ and adjacent areas of the base material, while compressive RS is presented in farther regions. Definite stress gradient exists in the vicinity of weld toe or weld root due to the steep temperature gradient as well as the effect of yield strength. The magnitude of residual stresses is decreased in far areas as there is lower effect of thermal cycle loads.

For the welded structure with the first type of weld joint in Fig. 4 (type 1), the RS profiles on the top surface are the same as that of the down surface of the plate (line type 1-top and type 1-down in Fig. 8) because the thickness of plate used here is relatively small ($t = 3$ mm). From the Figs. 8 and 9, the axis-symmetrical distribution of longitudinal RS is found due to the same material properties and geometric structure.

However, great differences can be found in the next two types of welded structures (type 2 and type 3). The longitudinal RS profiles on the thick plates ($t = 6$ mm) are portrayed in Fig. 8, and they are different between top and bottom surfaces of each plate thickness. The magnitude of RS on the transition surface is smaller than that of the other side face in each plate thickness due to the effect of geometric design of transition in thickness, which gradually increases with distance from the heat source. The difference found in the second butt-weld plate (type 2) is more definite than that of the other two welded structures (type 1 and type 3). It can be conducted that more

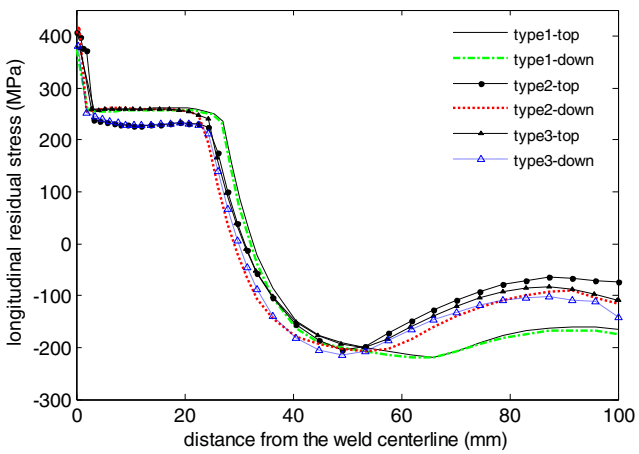

Fig. 8 Longitudinal residual stresses on the thick stainless plates

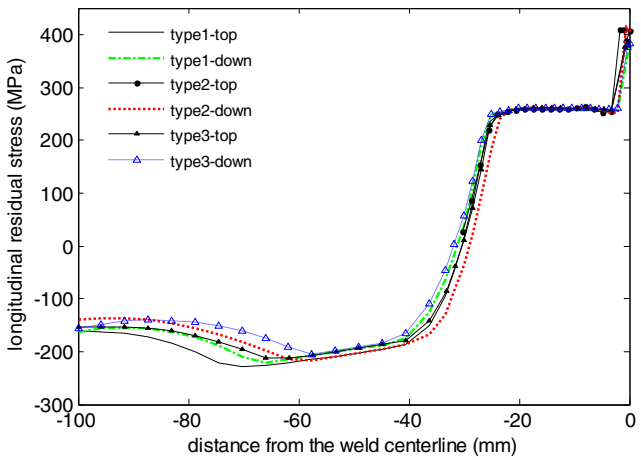

Fig. 9 Longitudinal residual stresses on the thin stainless plates

severe distortion occurs in the second weld plates (type 2) compared with that of the other two types of weld structures.

To the thick plates in two types of welded structures (type 2 and type 3), the residual stresses on the surfaces without slopes for transition in weld joints (type 2-down and type 3-top) show similar magnitude and distribution with that of type 1 in regions close to the weld bead for the dominating effect of high temperature. Similar RS profiles can be found on the slope surfaces for transition in the latter two types of welded structures (type 2 and type 3), although the slope faces are located at the weld toe and weld root side. In the farther area of base metal, the value of RS is decreased to some extent for the relatively weak effect of thermal cycle load and influence of plate thickness (thick plates for type 2 and type 3 is 6 mm, type 1 is 3 mm), which is a significant factor for the formation of RS [24].

Figure 9 provides the RS on the thin plates that connected with the thick plates, and also depicts the left plate in welded structure with the first type of weld joint (type 1). The results conclude that the longitudinal residual stresses on the thin plates in three types of welding structures show similar magnitude and distribution in the vicinity of weld filler.

4.4 Longitudinal RS profiles along the weld direction

The magnitude and distribution longitudinal RS along the weld direction are presented in Figs. 10 and 11 respectively. The selected points are located at positions 12 mm away from the weld center line. For the welded structure with the first type of joint (type 1), the thickness of both weld plates is 3 mm, and there is no significant difference for the RS profiles on the top and down surface of connected plates. Thereby, only the RS on the top face of the plate is depicted in the next two figures. The magnitudes and distributions of longitudinal residual stresses on both sides of weld filler are similar. At the

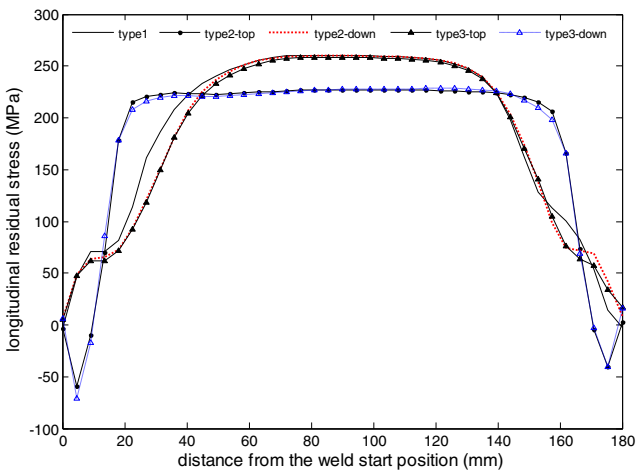

Fig. 10 Longitudinal residual stresses along the weld line for thick stainless plates (distance from the weld centerline is 12 mm)

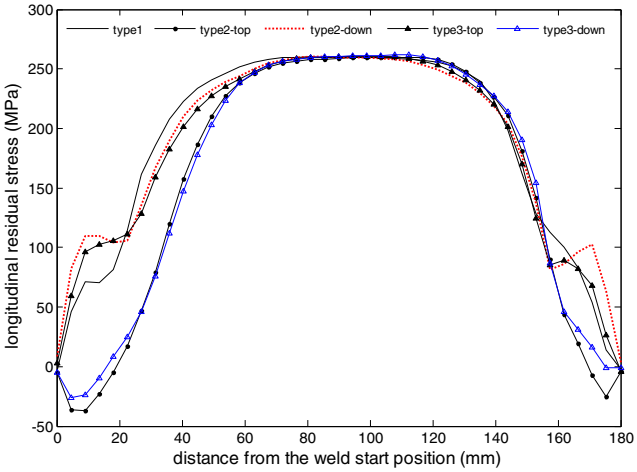

Fig. 11 Longitudinal residual stresses along the weld line for thin stainless plates (distance from the weld centerline is 12 mm)

start and stop positions, RS is released as no mechanical boundary constraint here. The RS formation lies in the center part of welded structure suffers the constraint of surrounding cold base metal.

The RS distribution on the thick plate along the weld center line is portrayed in Fig. 10. For the second and third types of welded structure (type 2 and type 3), similar RS properties can be found on their transition surfaces as well as surfaces without slope respectively. The RS on the top and down faces could be differentiated due to different geometric details. The longitudinal RS on the transition face shows a larger range of distribution compared with that of the other side face. Because of the geometric details at the location where thickness starts to change, there is a higher stiffness in the direction perpendicular to the steel plate. It also restrains the RS release at weld start/stop side of plates and leads to compressive RS (Fig. 10). However, this effect of constraint at both ends of the plate does not appear on other the faces without a transition slope. Since the transition faces on the thick plates are relatively far away from the heat source, the magnitude of RS is reduced to some extent for the lower influence of thermal cycle loads.

Figure 11 shows the longitudinal RS distribution on the thin steel plates in a similar manner to that used in Fig. 10. It can be conducted so that similar magnitudes and distributions are obtained from the thin plates of welded structures (type 1 and type 3). However, some differences occur at the two sides of plates due to the geometric details of the weld joint. More significant differences can be found in the second type of welded structure (type 2) for the more severe angular distortion induced by welding, and the magnitude of RS is reduced to some extent.

According to the comparative study on the three types of welding structures, it can be deduced that the axis-symmetrical magnitude and distribution of longitudinal RS

can be obtained from the first type of welded structure (type 1) because both the welding base metals have the same material properties and geometric structures. Butt-welded structures with steel plates of dissimilar thickness lead to the significant change of RS formation and distortion because the welding of such dissimilar joints needs geometric design in thickness direction, which partly changes the stiffness of the thick plate and surface distance from the heat source in the transitional region. The variation of the mechanical behavior and RS profiles on such dissimilar welded joints would be caused by non-uniform thermal loadings and different stiffness. The magnitude and distribution of RS is formed under the influence of the weld joint details and thickness of the plates. From the view of failure, the initial defect may grow into cracks and cause damage under fatigue loading and RS. The welding flaw and the concentration of severe stress mostly exist at the weld toe. Compared to the third type of weld joint, the second type of weld joint may be a better choice for the welding design of dissimilar thickness plates for relatively lower tensile RS.

5 Conclusions

Based on the thermal elastic-plastic FE technology, the weld-induced RS profiles and effects of geometric details of weld joints are carried out in this work. The conclusions can be deduced as follows:

For welded structures with joint type 1, the axis-symmetrical longitudinal RS could be found on both sides of the weld bead because of the similar geometric components and material properties.

The magnitudes and distributions of RS are deeply influenced by the geometric details of weld joints and base materials. For the dissimilar weld joints (type 2 and type 3), the longitudinal RS and distortion of thick plates are different from that of thin plates. The value of RS for thick plates is reduced to some extent due to the effect of plate thickness. In the transitional face region, the longitudinal RS is somewhat reduced due to the incremental distance from the heat source with regards to thickness. Since the greater stiffness at the position of transition face is reinforced, longitudinal RS along the weld direction distributes a larger region on the plate. Compressive RS also appears at the region close to weld start/stop position. The effect of thicknes on the RS under the same welding conditions can be deduced in this work. The value of RS on thick plate is smaller than that of thin components because of the dominating effect of thickness and less thermal cycle load in this area.

Acknowledgments The research was supported by the National Natural Science Foundation of China (51438002, 51108075, 51578137), Open Research Fund Program of Jiangsu Key Laboratory of Engineering Mechanics, and A Project Funded by the Priority Academic Program Development of the Jiangsu Higher Education Institutions.

References

1. Withers PJ (2007) Residual stress and its role in failure. Rep Prog Phys 70(12):2211–2264. doi:10.1088/0034-4885/70/12/R04
2. Lindgren LE (2006) Numerical modelling of welding. Comput Method Appl M 195(48–49):6710–6736. doi:10.1016/j.cma.2005.08.018
3. Deng D, Murakawa H (2008) Prediction of welding distortion and residual stress in a thin plate butt-welded joint. Comp Mater Sci 43(2):353–365. doi:10.1016/j.commatsci. 2007.12.006
4. Lee CH, Chang KH (2007) Numerical analysis of residual stresses in welds of similar or dissimilar steel weldments under superimposed tensile loads. Comp Mater Sci 40(4):548–556. doi:10.1016/j.commatsci.2007.02.005
5. Lee CH, Chang KH, Lee CY (2008) Comparative study of welding residual stresses in carbon and stainless steel butt welds. Proc I Mech Eng B-J Eng 222(12):1685–1694. doi:10.1243/09544054JEM1244
6. Eisazadeh H, Achuthan A, Goldak JA, Aidun DK (2015) Effect of material properties and mechanical tensioning load on residual stress formation in GTA 304-A36 dissimilar weld. J Mater Process Tech 222:344–355. doi:10.1016/j.jmatprotec.2015.03.021
7. Choobi MS, Haghpanahi M, Sedighi M (2010) Investigation of the effect of clamping on residual stresses and distortions in butt-welded plates. Sci Iran Transaction B-Mech Eng 17(5):387–394
8. Choobi MS (2013) Investigating the effect of geometrical parameters on distortions in butt- welded plates. J Strain Anal Eng 48(4):258–268. doi:10.1177/0309324713480766
9. Ranjbarnodeh E, Serajzadeh S, Kokabi AH, Hanke S, Fischer A (2011) Finite element modeling of the effect of heat input on residual stresses in dissimilar joints. Int J Adv Manuf Technol 55(5–8):649–656. doi:10.1007/s00170-010-3095-3
10. Okano S, Tanaka M, Mochizuki M (2011) Arc physics based heat source modelling for numerical simulation of weld residual stress and distortion. Sci Technol Weld Joi 16(3):209–214. doi:10.1179/1362171810Y.0000000019
11. Ye YH, Cai JP, Jiang XH, Dai DP, Deng D (2015) Influence of groove type on welding-induced residual stress, deformation and width of sensitization region in a SUS304 steel butt welded joint. Adv Eng Softw 86:39–48. doi:10.1016/j.advengsoft.2015.04.001
12. Singh S, Yadaiah N, Bag S, Pal S (2014) Numerical simulation of welding-induced residual stress in fusion welding process using adaptive volumetric heat source. P I Mech Eng C-J Mec 228(16):2960–2972. doi:10.1177/0954406214525601
13. Suzuki H, Katsuyama J, Morii Y (2012) Comparison of residual stress distributions of similar and dissimilar thick butt-weld plates. J Solid Mech Mater Eng 6(6):574–583. doi:10.1299/jmmp.6.574
14. Pouranvari M, Marashi SPH (2011) Dissimilar spot welds of AISI 304/AISI 1008: metallurgical and mechanical characterization. Steel Res Int 82(12):1355–1361. doi:10.1002/srin.201100139
15. Moat RJ, Stone HJ, Shirzadi AA, Francis JA, Kundu S, Mark AF, Bhadeshia HKDH, Karlsson L, Withers PJ (2011) Design of weld fillers for mitigation of residual stresses in ferritic and austenitic steel welds. Sci Technol Weld Joi 16(3):279–284. doi:10.1179/1362171811Y.0000000003
16. Jiamin S, Xiaozhan L, Yangang T, Deng D (2014) A comparative study on welding temperature fields, residual stress distributions and deformations induced by laser beam welding and CO2 gas

arc welding. Mater Design 63:519–530. doi:10.1016/j.matdes.2014.06.057
17. Deng D, Kiyoshima S (2012) Numerical simulation of welding temperature field, residual stress and deformation induced by electro slag welding. Comp Mater Sci 62:23–34. doi:10.1016/j.commatsci.2012.04.037
18. Hashemzadeh M, Chen BQ, Guedes Soares C (2015) Numerical and experimental study on butt weld with dissimilar thickness of thin stainless steel plate. Int J Adv Manuf Technol 78(1–4):319–330. doi:10.1007/s00170-014-6597-6
19. Brickstad B, Josefson BL (1998) A parametric study of residual stresses in multi-pass butt- welded stainless steel pipes. Int J Pres Pip 75(1):11–25. doi:10.1016/S0308-0161 (97) 00117-8
20. Goldak J, Chakravarti A, Bibby M (1984) A new finite element model for welding heat sources. Metall Trans B 15(2):299–305. doi:10.1007/BF02667333
21. CWS Welding handbook (vol.3). The Chinese mechanical engineering society welding society. China machine press, China in Chinese
22. Goldak J, Akhlaghi M (2006) Computational welding mechanics. Springer Science & Business Media
23. Akhlaghi FZ (2014) Welding simulation and fatigue assessment of tubular K-joints in high-strength steel. Dissertation. Ecole Polytechnique Fédérale de Lausanne
24. Seyyedian M, Amini S, Haghpanahi M (2009) Study of the effect of thickness on residual stresses in butt welding of SUS304 plates. IIW International Conference on Advances in Welding and Allied Technologies, Singapore 17(5):195–200